Glaciers of North America–

GLACIERS OF CANADA

GLACIERS OF THE ST. ELIAS MOUNTAINS

By GARRY K.C. CLARKE *and* GERALD HOLDSWORTH

With a section on QUANTITATIVE MEASUREMENTS OF TWEEDSMUIR AND LOWELL GLACIER IMAGERY

By GERALD HOLDSWORTH, PHILIP J. HOWARTH, *and* C. SIMON L. OMMANNEY

SATELLITE IMAGE ATLAS OF GLACIERS OF THE WORLD

Edited by RICHARD S. WILLIAMS, Jr., *and* JANE G. FERRIGNO

U.S. GEOLOGICAL SURVEY PROFESSIONAL PAPER 1386–J–1

The St. Elias Mountains, which straddle the Canadian and U.S. border, are highly glacierized; ice fields and associated outlet glaciers, plateau glaciers, valley glaciers, and piedmont glaciers are common. The mix of sub-polar and cold glaciers range in area from a few km^2 to more than 1200 km^2 (Seward Glacier). At least 136 of the sub-polar glaciers are surge-type glaciers; the looped medial moraines of surging glaciers are distinctive features on Landsat images. The dynamics of two surging glaciers, Tweedsmuir and Lowell Glaciers, are analyzed on sequential Landsat images

CONTENTS

GLACIERS OF NORTH AMERICA–

GLACIERS OF CANADA

GLACIERS OF THE ST. ELIAS MOUNTAINS

By GARRY K.C. CLARKE[1] *and* GERALD HOLDSWORTH[2]

With a section on QUANTITATIVE MEASUREMENTS OF TWEEDSMUIR GLACIER AND LOWELL GLACIER IMAGERY
By GERALD HOLDSWORTH,[2] PHILIP J. HOWARTH,[3] *and* C. SIMON L. OMMANNEY[4]

Abstract

The St. Elias Mountains region of Canada is made up of a series of mountain ranges that contain a particularly wide variety of glacier types, defined both morphologically and thermally. This variety is a result of the extreme topography, which has a maximum relief of 4,200 meters within a few kilometers, coupled with the large gradients recorded in precipitation and temperature throughout the ranges. Glacier types seen here are valley glaciers, high-elevation plateau glaciers, ice fields and associated outlet glaciers,[5] and piedmont glaciers of different shapes and sizes. Glacier lengths range from about a kilometer to more than 70 kilometers (Hubbard Glacier, which ends in Alaska, has a length of 72 kilometers in Canada and a total length of 112 kilometers); their areas range from a few square kilometers to more than 1,200 square kilometers for Seward Glacier. Temperate glaciers are common at low elevations, particularly on the Pacific Ocean side of the axis (drainage divide). Subpolar glaciers are present on the north (continental) side of the axis even at low elevations. Cold glaciers, at "polar" temperatures, exist on high-elevation plateaus such as on Mount Logan (5,956 meters). The presence of a large concentration of generally subpolar surging glaciers in the region is particularly noteworthy. This topic receives the most attention here because features diagnostic of surges are easily detected on satellite images, from which time-series measurements, related to the dynamics of the glacier, may be made, as shown for Tweedsmuir Glacier and Lowell Glacier.

Introduction

The St. Elias Mountains, straddling the international border between Alaska and Canada (fig. 1), are among the world's most rugged and spectacular glacierized landscapes. This is a region of great scientific interest, particularly to the glaciologist, because few other areas combine such a

Manuscript approved for publication 7 March 2002.

[1] Department of Earth and Ocean Sciences, University of British Columbia, 6339 Stores Road, Vancouver, British Columbia V6T 1Z4, Canada.

[2] Arctic Institute of North America, University of Calgary, 2500 University Drive, NW., Calgary, Alberta T2N 1N4, Canada; Institute for the Study of Earth, Oceans, and Space, Morse Hall, University of New Hampshire, Durham, NH 03824–3525; and the National Hydrology Research Centre, 11 Innovation Boulevard, Saskatoon, Saskatchewan S7N 3H5, Canada; e-mail address: [gholdswo@acs.ucalgary.ca].

[3] Department of Geography, University of Waterloo, Waterloo, Ontario N2L 3G1, Canada.

[4] International Glaciological Society, Lensfield Road, Cambridge CB2 1ER, England, U.K. (formerly with the National Hydrology Research Institute [now the National Hydrology Research Centre], 11 Innovation Boulevard, Saskatoon, Saskatchewan S7N 3H5, Canada).

[5] In Canada, icefield is commonly used in place-names instead of ice field. In the volumes of the Satellite Image Atlas of Glaciers of the World, ice field is used (compare Jackson, 1997, p. 316) in the glaciological sense of the term.

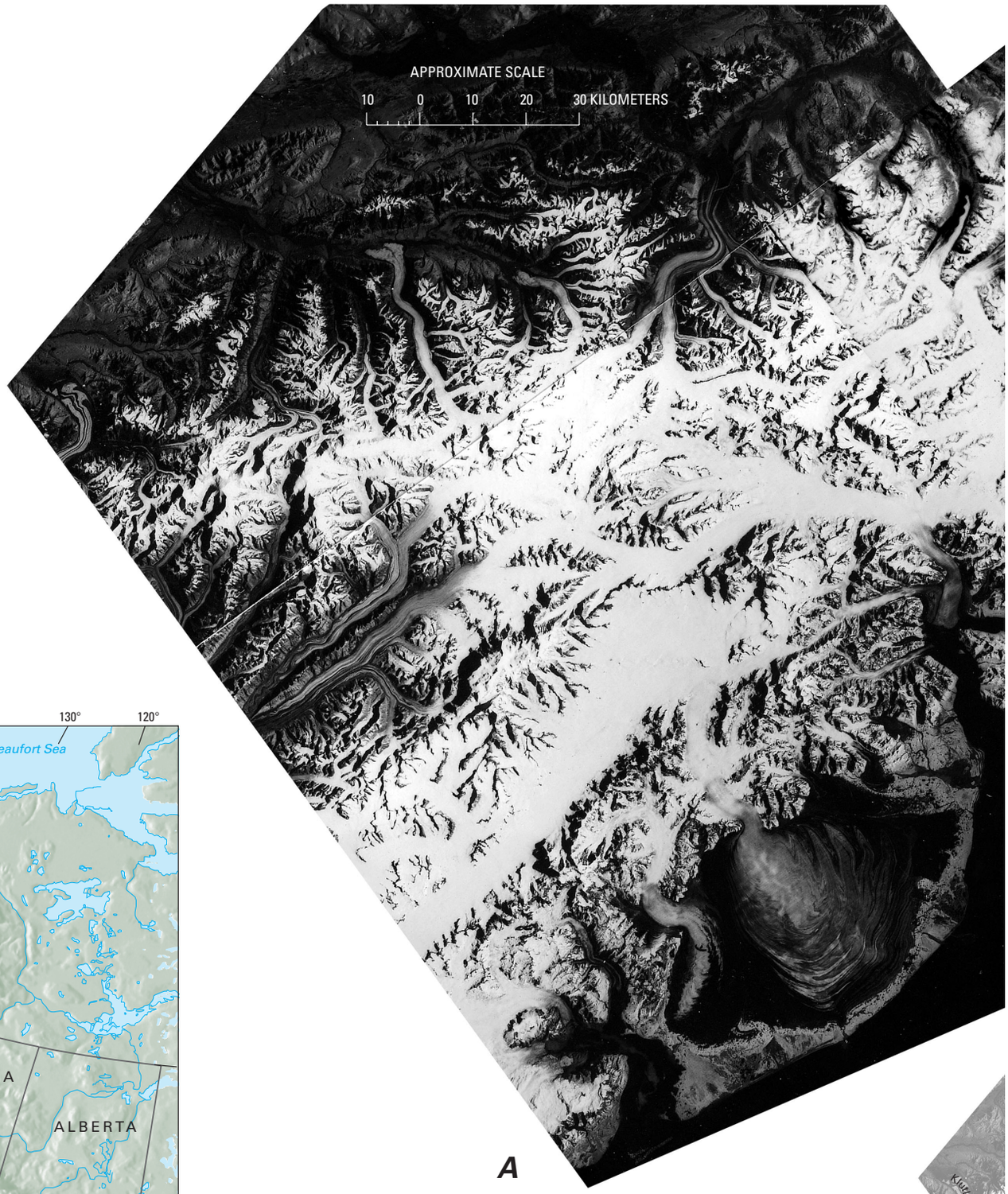

Figure 1.—*Location of the St. Elias Mountains, Yukon Territory-Alaska, and Landsat image mosaics of the mountains.* **A**, *Landsat 2 and 3 multispectral scanner (MSS) image mosaic of the St. Elias Mountains. Landsat images (21314–19295, band 7; 28 August 1978; Path 66, Row 18; 2952–19124, band 7; 31 August 1977; Path 64, Row 19; 2955–19285 and 2955–19292, band 7; 3 September 1977; Path 67, Rows 17 and 18; 3157–19514, band 7; 23 June 1982; Path 66, Row 18) are from the EROS Data Center, Sioux Falls, S. Dak.* **B**, *Annotated Landsat 2 and 3 MSS image mosaic of the St. Elias Mountains using the same Landsat images as for* A. *Abbreviations: Gl., Glacier; Mt., Mount; Mtn., Mountain; N., North; S., South.*

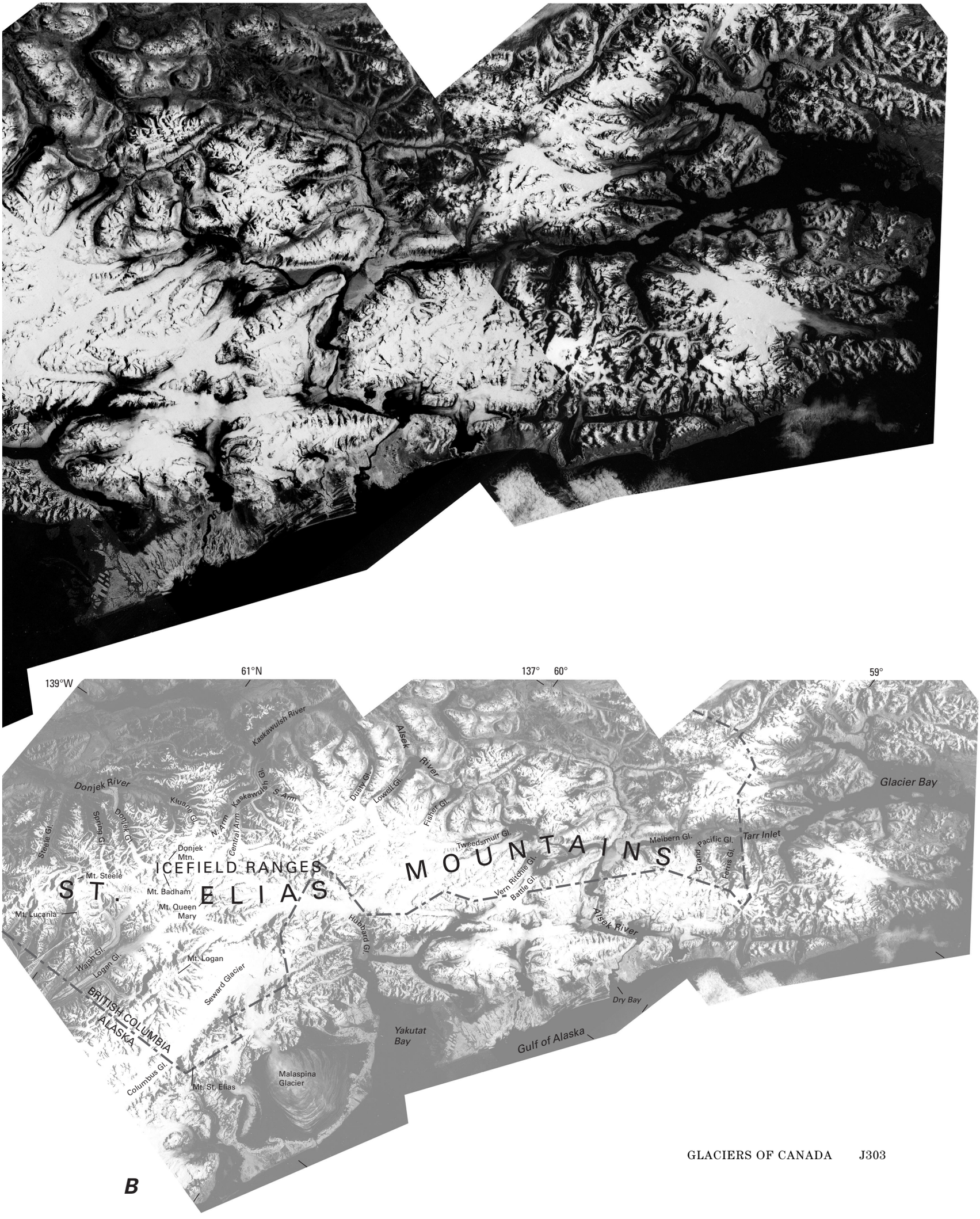
139°W
61°N
137°
60°
59°
Kaskawulsh River
Donjek River
Kluane Gl.
N. Arm
Central Arm
Kaskawulsh Gl.
S. Arm
Donjek Gl.
Spring Gl.
Steele Gl.
Donjek Mtn.
Mt. Steele
ICEFIELD RANGES
ST. ELIAS
Mt. Badham
Mt. Queen Mary
Mt. Lucania
Walsh Gl.
Logan Gl.
Mt. Logan
Seward Glacier
BRITISH COLUMBIA
ALASKA
Columbus Gl.
Mt. St. Elias
Malaspina Glacier
Yakutat Bay
Gulf of Alaska
Dry Bay
Alsek River
Dusty Gl.
Lowell Gl.
Fisher Gl.
Hubbard Gl.
Tweedsmuir Gl.
Vern Ritchie Gl.
Battle Gl.
MOUNTAINS
Melbern Gl.
Grand Pacific Gl.
Ferris Gl.
Tarr Inlet
Glacier Bay

B

concentration of glaciers with such a wide variety of glacier types. The explanation for both the concentration and the variety lies in the region's proximity to the Gulf of Alaska and in the large elevation change found between the Alaskan coast and the central axis of the mountain ranges that make up the St. Elias Mountains. In fact, the elevation rises within a few kilometers of the coast to a maximum relief of 4,200 m. Some of the highest precipitation rates in Canada are present in this region, and snow may fall at any time of the year.

The Icefield Ranges (fig. 2) form the central axis or crest of the St. Elias Mountains and act as both a hydrologic and climatic divide. This is the region of the most intense glacier activity and the location of the highest peaks: Mount Logan (5,956 m, labeled 1 in fig. 2), Canada's highest mountain; Mount St. Elias (5,489 m, labeled 2 in fig. 2); Mount Lucania (5,227 m, labeled 21 in fig. 2), and Mount Steele (5,067 m, labeled 22 in fig. 2). The topographic barrier formed by the Icefield Ranges imposes a strong gradient in precipitation and mean annual temperature from the Alaskan coast to the edge of the Yukon interior. Glaciers, representing every geophysical class from temperate to cold (high polar), are found here. In general, temperate glaciers are common at low elevations, particularly on the Pacific Ocean side of the axis (drainage divide). Subpolar glaciers are present on the north (continental) side of the axis even at low elevations. Temperatures, as measured at 10 m depth in the firn, range from 0°C on the Seward Glacier (labeled 17 in fig. 2) at 1,800 m (Sharp, 1951b) to about –29°C on Mount Logan at 5,340 m (Holdsworth and others, 1992). Some glaciers are subpolar in their ablation areas and temperate elsewhere; others are apparently temperate in their ablation areas and slightly cold on their névés. An example of this is the transect glacier system of Kaskawulsh and Hubbard Glaciers (labeled 12 and 18 in fig. 2) which share a common divide at 2,674 m.

A remarkable feature of the valley glaciers of the St. Elias Mountains is that so many of them surge (Meier and Post, 1969). Of the 204 surging glaciers identified by Post (1969) in western North America, 136 are in the St. Elias Mountains, and most of these are in Canada. The most important, generally subpolar, surging glaciers located entirely or partly in the Canadian part of the St. Elias Mountains are the Anderson (labeled 6 in fig. 2), Chitina (5), Walsh (4), Klutlan (7), Steele (8), Donjek (10), Kluane (11), Dusty (13), Lowell (14), and Tweedsmuir Glaciers (fig. 1). The surging character of most of these glaciers can easily be identified by the characteristically looped medial moraines that can be seen so well on Landsat imagery. Whereas it is striking that so many of the very large glaciers surge, size alone is not the key to understanding surges because many medium-sized and even very small glaciers surge (Clarke, 1991). Also, no one obvious explanation exists for the remarkable geographical concentration of surging glaciers in the St. Elias Mountains. [For a discussion of surging glaciers, the reader is referred to Chapter K, Glaciers of Alaska; see also Chapter E, Glaciers of Svalbard, Norway, another glacierized region that has a variety of glacier types and a large number (86) of surging glaciers documented from the end of the 19th century to 1993.]

The following commentary discusses the major glaciers in the region and, following Field (1975), is organized according to recognized hydrologic-drainage systems. Glacier lengths have been measured from current (usually 1:250,000-scale) topographic maps and are given in square brackets, although some discrepancies are present between the values given here and those given by Field (1975). Glacier lengths range from about a kilometer to more than 70 kilometers (Hubbard Glacier, which ends in Alaska, has a length of 72 kilometers in Canada and a total length of 112 kilometers); their areas range from a few square kilometers to more than 1,200 square kilometers for Seward Glacier.

Figure 2.—*(opposite page) Annotated mosaic of Landsat 2 MSS images of the Icefield Ranges, St. Elias Mountains, Yukon Territory-Alaska. Annotations: 1, Mount Logan (elevation 5,956 m), highest mountain in Canada; 2, Mount St. Elias (elevation 5,489 m), second highest mountain in Canada; 3, Logan Glacier; 4, Walsh Glacier; 5, Chitina Glacier; 6, Anderson Glacier; 7, Klutlan Glacier; 8, Steele Glacier; 9, Spring Glacier; 10, Donjek Glacier; 11, Kluane Glacier; 12, Kaskawulsh Glacier; 13, Dusty Glacier; 14, Lowell Glacier; 15, Fisher Glacier; 16, Malaspina Glacier; 17, Seward Glacier; 18, Hubbard Glacier; 19, Russell Fiord; 20, Columbus Glacier; 21, Mount Lucania; 22, Mount Steele. The Landsat images (2955–19285 and 2955–19292, band 7; 3 September 1977; Path 67, Rows 17 and 18) are from the EROS Data Center, Sioux Falls, S. Dak. Map reference: Mount St. Elias map sheet 115B and 115C, 1:250,000 scale.*


140°W
139°
138°
141°W
61°N
60°
Kluane Lake
ICEFIELD RANGES
1
2
3
4
5
6
7
8
9
10
11
12
13
14
15
16
17
18
19
20
21
22
APPROXIMATE SCALE
0
50 KILOMETERS

Most of the glaciers discussed are of the valley type. However, another important class of glaciers is mentioned here because of its relevance to ice coring. These are the high-elevation plateau glacier systems such as on Mount Logan (fig. 1). They are in the permanent accumulation area and thus appear white on satellite images throughout the year. In addition, ice fields and piedmont glaciers are found here as well.

Chitina River Valley System

The major glaciers of the Chitina River valley system are the Anderson [40 km], Chitina [70 km], Walsh [70 km], and Logan [70 km] Glaciers (fig. 3). All have their accumulation zones in the Icefield Ranges of Canada and flow across the 141st meridian, which defines the border between the Yukon Territory and Alaska. In the recent past, these glaciers were tributaries of a large trunk glacier that occupied the upper Chitina River valley. On the 1975 National Topographic Series (NTS) map sheet 115SW and 115SE (1:500,000 scale), these four glaciers are seen to merge. Now, the

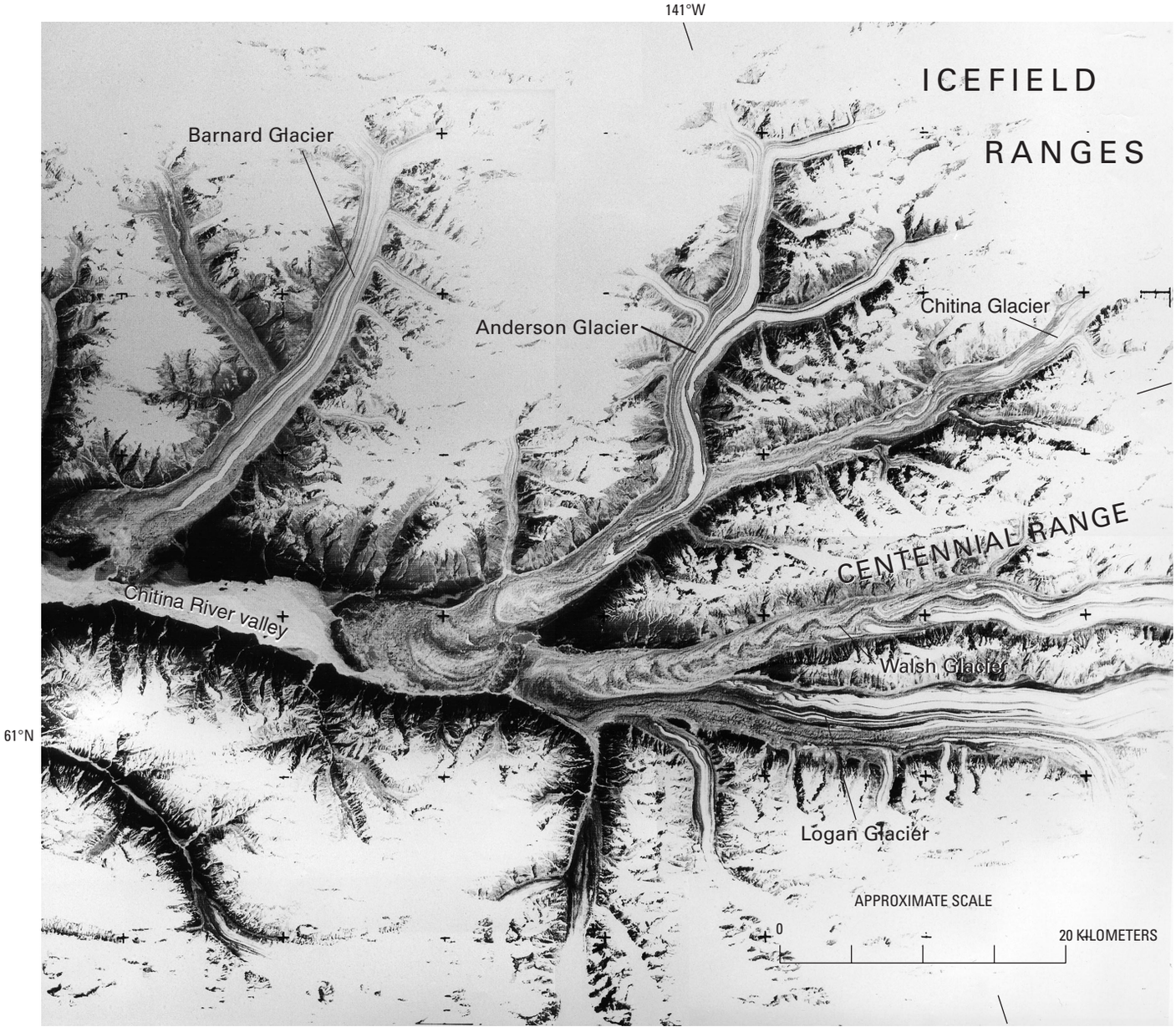

Figure 3.—*Annotated enlargement of part of a Landsat 3 return beam vidicon (RBV) image showing the glaciers of the upper Chitina River valley basin, St. Elias Mountains, Yukon Territory-Alaska. Walsh Glacier shows well-defined moraine loops that identify the glacier as surging. Its 1960–64 surge displaced ice as much as 11.5 km—a record for North America. The approximate 1968 surge of Anderson Glacier truncated the terminus of Chitina Glacier, another surging glacier. Logan Glacier is not included in Post's (1969) catalog of surging glaciers; the moraine loops near its confluence with Walsh Glacier indicate variations in flow velocity, but these may be in response to surges of Walsh Glacier. The Landsat 3 RBV image (30853–19510; 5 July 1980; Path 68, Row 17, Subscene C) is archived by the U.S. Geological Survey Glacier Studies Project. Map references: Kluane Lake map sheet 115G and 115F (E 1/2); Mount St. Elias map sheet 115B and 115C; Bering Glacier map sheet N6000–W14100/60x180; McCarthy map sheet N6100–W14100/60x180; all 1:250,000 scale.*

Logan-Walsh merger and the Anderson-Chitina merger do not appear to connect with each other. The glacier system also does not appear to merge on two satellite images taken 3 years apart (Landsat 1, 7 August 1974; Path 69, Row 17; and 4 September 1977; Path 68, Row 17). However, inspection of a later image (Landsat image, 1 Nov 1978; Path 68, Row 17, the same scene illuminated by a low (13°) Sun angle on thin snow cover) shows that a (1- to 1.5-km) section of ice-cored moraine probably still bridges the two glacier pairs. The same pitted surface topography that is characteristic of the terminus of all the glaciers is also seen in that section. The glaciers look essentially the same on the three images, which indicates that they were in a quiescent phase.

A surge of Walsh Glacier, thought to have started in late 1960 or early 1961, lasted 4 years and displaced ice as much as 11.5 km—a record for North America (Post, 1966, 1967). Conspicuous medial moraine loops can be traced on the glacier surface, and their spacing can be used to infer a fairly regular surge-cycle periodicity for Walsh Glacier. Note that the Walsh Glacier apparently overrides the end of Logan Glacier (fig. 3). In 1966, the Anderson Glacier showed signs of entering a surge phase (Post, 1967) and was observed to be surging in 1968. It was reported (Field, 1975) that the surge was slowing down in early 1971. Landsat images of 1974, 1977, and 1980 (see fig. 3) show the Chitina Glacier totally overridden by the Anderson Glacier surge.

White River Valley System

Klutlan Glacier (fig. 1) [approximately 72 km measured from the base of Mount Bona, Alaska] is a large surging glacier that has numerous tributaries feeding ice into it. Only the last 25 km of the glacier is in Canada where it has two important tributaries entering it on the south side. These are the Nesham and Mount Wood Glaciers—both of which surge. On the Landsat images, evidence of surging of the Klutlan is seen only below the Nesham Glacier, despite Field's claim that "the entire Klutlan system is subjected to repeated surges" (Field, 1975). The same Landsat images of 7 August 1974 (Path 69, Row 17) and 4 September 1977 (Path 68, Row 17) mentioned above show virtually no change in configuration of the lower glacier or of the tributaries, so the system was in the quiescent phase then. Field (1975) states that "a small left-hand tributary of the Nesham surged independently in 1966." The end of the glacier is quite indistinct, and ice-cored moraine may stretch more than 12 km beyond the last visible white ice. Recent surges have not disturbed this terminal area, and a spruce forest has grown up on the moraine cover. Past major surges blocked regional drainage and formed glacier-dammed lakes; two of these lakes had estimated volumes exceeding 10^8 m^3. The catastrophic emptying of these lakes might have produced substantial jökulhlaups (glacier-outburst floods) in the White River valley. The glacial geology and paleolimnology of this lower deglaciated region have received considerable attention (Rampton, 1970; Bradbury and Whiteside, 1980; Driscoll, 1980; Whiteside and others, 1980; Wright, 1980).

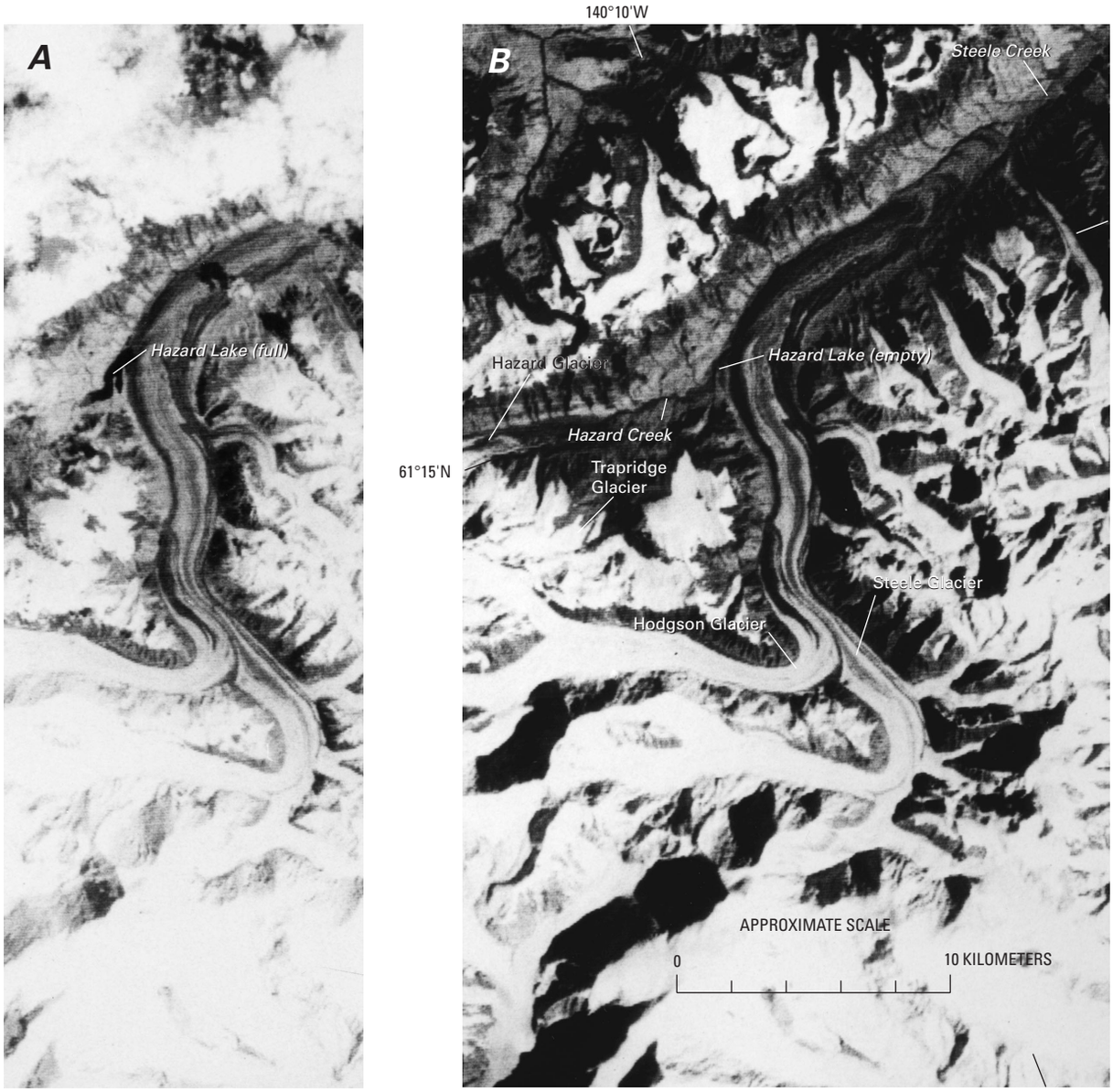

Donjek River Valley System

Steele Glacier [approximately 40 km long] is best known for its 1965–66 surge. Figure 4 shows the glacier in its quiescent phase. Note that the large western tributary apparently overrides the southeast, or main, trunk of the glacier. This feature is a relict of the surge a decade earlier. The ice-cored moraine of the overextended lower glacier, now shrunken, can also be clearly seen. Steele Glacier was one of the few glaciers in the region to receive early scientific attention (Sharp, 1943, 1951a; Wood, 1936, 1942, 1972). A minor surge in the early 1940's did not affect the lower glacier. The last surge, in contrast, was quite spectacular. It started in late 1965, and by summer 1966, a large wavelike bulge was seen moving down the glacier. By summer 1967, the total ice displacement was as much as 9.5 km (Stanley, 1969). The peak speed during the approximately 3-year duration of the surge phase was 24 m d^{-1}, reached in early 1966. By the beginning of 1968, the speed was down to 1 m d^{-1} and dwindling. Between surges, the lower (ablation) zone is virtually stagnant, and the ice is covered by rock debris. The Steele Glacier and several of the smaller glaciers (such as Trapridge Glacier) in the Steele Creek drainage basin are known to be subpolar;

Figure 4.—*Annotated enlargements of parts of two Landsat 2 MSS images showing glaciers of Steele Creek drainage basin, Yukon Territory. Steele Glacier surged in 1965-66, and displaced ice as much as 9.5 km, which dammed Hazard Creek in the process. The resulting proglacial lake, known as Hazard Lake, now fills and drains annually. A surge of Hodgson Glacier, a tributary of the Steele, followed the Steele surge by several years and may have been triggered by it.* **A**, *A part of Landsat image 2901–19315, band 7; 11 July 1977; Path 67, Row 17, showing glacier-dammed Hazard Lake full and partial cloud cover.* **B**, *A part of Landsat image 2955–19285, band 7; 3 September 1977; Path 67, Row 17, showing the empty basin of Hazard Lake after an outburst flood that took place between 2 and 5 August 1977. The lake drains through a subglacial tunnel that runs from the ice dam to the Steele Glacier terminus at the head of Steele Creek. The Landsat images are from the EROS Data Center, Sioux Falls, S. Dak. Map reference: Kluane Lake map sheet 115G and 115F (E 1/2), 1:250,000 scale.*

hence, it is postulated that their surge mechanism is thermally controlled (Jarvis and Clarke, 1974, 1975, and Clarke and Jarvis, 1976).

The 1965 surge dammed Hazard Creek and created Hazard Lake on the left margin of Steele Glacier near the sharp bend in the glacier. This lake is a transient feature that disappears entirely when the ice level ablates sufficiently. During the 1970's and 1980's, the annual cycle of filling and self-draining of the lake was studied in detail (Collins and Clarke, 1977; Clarke, 1982). The draining of the lake generated small (600 m^3 s^{-1}) jökulhlaups in Steele Creek. Figure 4*A* shows the lake full on 11 July 1977; figure 4*B* shows it empty on 3 September 1977 following the draining of 2–5 August 1977.

Southeast of Steele Glacier are the following glaciers: Spring [approximately 26 km long], Donjek [55 km], and Kluane [35 km] Glaciers (fig. 5). All are known to surge, but only the Donjek has received much attention. The Donjek Glacier terminus spreads out as it flows into a river valley to form a small piedmont lobe. Former (major) surges have caused this lobe to expand and to butt against the Donjek Ranges to the east, which blocked the flow in the river that is fed by Kluane Glacier and numerous other smaller glaciers to the east.

Just prior to July 1974, the last tributary on the southeast margin of Donjek Glacier surged. A Landsat image of 15 September 1973 (Path 67, Row 17) shows the presurge condition, and an image of 4 September 1977 (Path 68, Row 17) shows the relict effect of the surge on the main glacier 3 years after the event (also see fig. 5, 10 August 1980). Donjek Glacier did not respond to the surge. In 1978, a minor surge of Donjek Glacier failed to dam the river. Several centuries ago, the glacier formed an ice dam that created Lake Donjek, estimated to have had a volume of 230 $x10^6$ m^3 (see lake site in fig. 5). This transient lake was thought to have drained catastrophically on at least one occasion (Clarke and Mathews, 1981). The terminal moraines of this glacier have been studied by Johnson (1972a, b).

In one of the major accumulation basins of the Donjek Glacier, between Donjek Mountain and Mount Badham, is an ice-core drill site, referred to in the literature (for example, Holdsworth and Peake, 1985) as *Eclipse*. The site is at lat 60°50'N., long 139°50'W. at an elevation of 3,017 m (maps 115B and 115C, Mount St. Elias map sheet, 1:250,000 scale) and has been core drilled on several occasions. Here, the 10-m firn temperature is –6°C, which makes this part of the glacier subpolar. The mean annual air temperature here is –13°C, as determined from an automatic weather station (Holdsworth, 1992). The annual accumulation rate is determined from pit and core studies to be 1,500 kg m^{-2} a^{-1} (1,500 mm water equivalent). The depth of ice as determined by radar is about 550 m. The site awaits deep drilling in order to acquire a long ice core.

Slims River Valley System

Kaskawulsh Glacier [75 km long] (fig. 6) flows from a divide that it shares with the Hubbard Glacier (fig. 1) and ends at the head of two river valleys: the Slims and the Kaskawulsh. Thus, the glacier contributes water to two rivers simultaneously; the relative contributions, which vary from year to year, depend on snout position and varying hydrologic-sedimentation conditions. Although Slims River now flows into Kluane Lake (fig. 2), in earlier times, Kluane Lake drained through the (reversed) Slims River down the Kaskawulsh River and into the Alsek River (fig. 1) (and thence to the Pacific Ocean) (Bostock, 1969). Kaskawulsh Glacier is not known to surge, and this is confirmed by the regular pattern of medial moraines seen in satellite images (fig. 6). However, the last tributary flowing into the *central arm* contains wavy moraines and a "beaded" suture, indicating that this tributary has surged at least once in

Figure 5.—*Annotated enlargement of part of a Landsat 3 MSS image showing the Donjek Glacier region, St. Elias Mountains, Yukon Territory. Spring, Donjek, and Kluane Glaciers are surge-type glaciers. Surges of Donjek Glacier have historically closed the Donjek River channel near Mount Hoge to form a large lake. An outburst flood from the lake could release roughly 230 x 10^6 m^3 of water across the Alaska Highway and the route of a proposed natural gas pipeline. A weak surge of Donjek Glacier, noted in 1978, almost dammed Donjek River. The Landsat image (30889–19492, band 7; 10 August 1980; Path 68, Row 17) is from the EROS Data Center, Sioux Falls, S. Dak. Map reference: Kluane Lake map sheet 115G and 115F (E 1/2), 1:250,000 scale.*

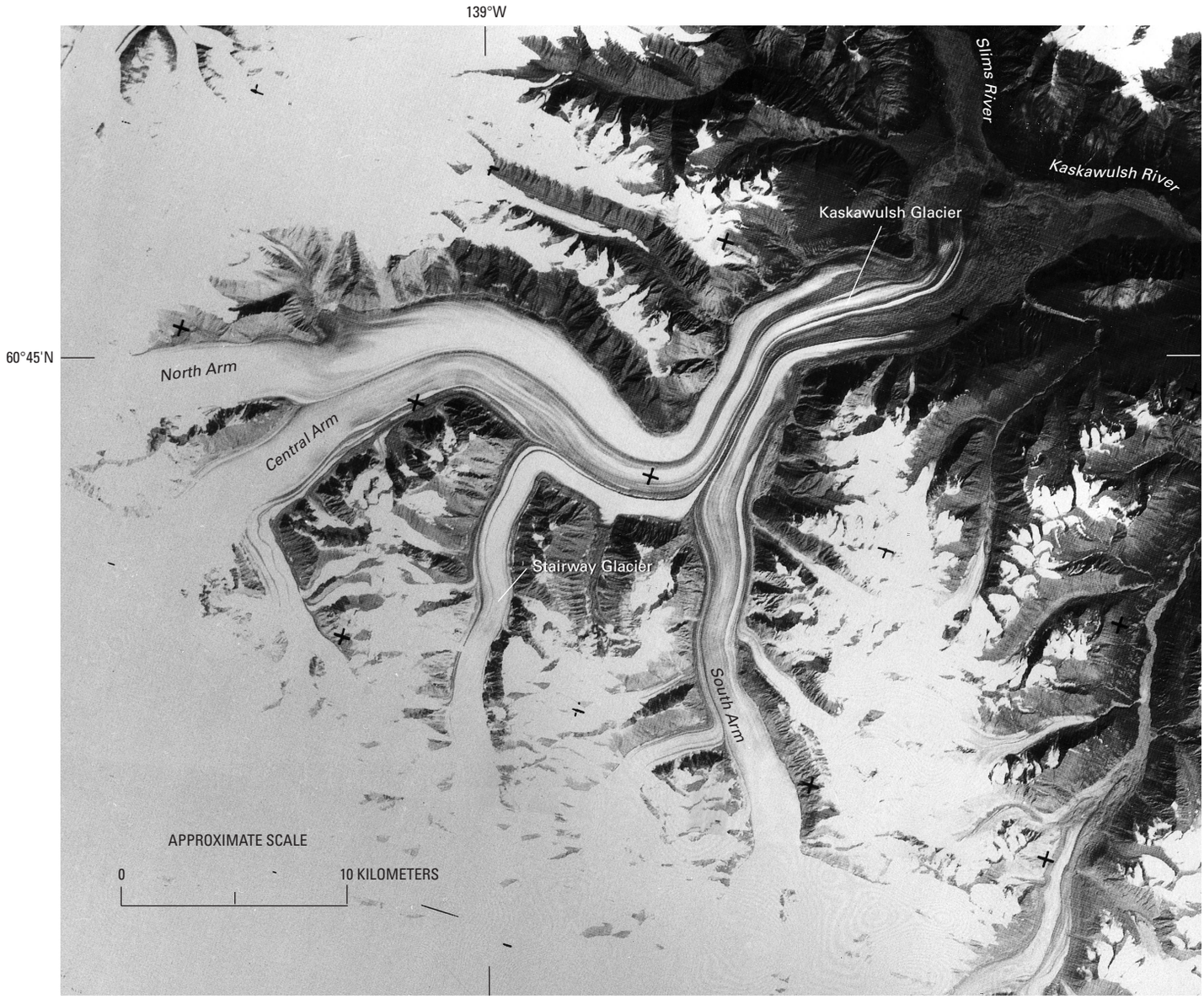

***Figure 6.**—Annotated enlargement of part of a Landsat 3 RBV image of Kaskawulsh Glacier, Yukon Territory. Kaskawulsh Glacier is one of the few large glaciers of the St. Elias Mountains that does not surge. It is a classic example of a trunk glacier that has many tributary branches. The uncontorted medial moraines indicate steady, rather than irregular, flow. The glacier terminus is at a major hydrologic divide, as Slims River flows to the Arctic Ocean and Kaskawulsh River flows to the Pacific Ocean. The Landsat 3 RBV image (30167–19491; 19 August 1978; Path 66, Row 18, Subscene A) is archived by the U.S. Geological Survey Glacier Studies Project. Map reference: Mount St. Elias map sheet 115B and 115C, 1;250,000 scale.*

the past. Low-altitude aerial photographs acquired in the 1970's and 1980's also suggest a similar conclusion. This is an example where surging tributaries do not necessarily trigger surges in the main glacier.

Measured ice thicknesses vary from 780 m near the divide (Clarke, 1967) to 650 m at the entrance to the *north arm* (Holdsworth, 1965) to 1,040 m in the ablation zone below the confluence of the *north* and *central arms* (Dewart, 1970). Surface-flow rates reach 150 m a^{-1} at the entrance to the *north arm* (Brecher, 1966) and have an ice discharge of more than 10^8 m^3 a^{-1} (Holdsworth, 1965). Ice-flow rates increase through an ice fall and then decrease to 179 m a^{-1} below the confluence (Dewart, 1970). Although some suggest that the divide region contains some "cold" firn [see Field (1975)], the general consensus is that the glacier is temperate. Holdsworth (1965) found that deep temperatures in partial water-filled crevasses at the entrance to the *north arm* are 0°C during the summer.

The intensity of research on the Kaskawulsh Glacier, and in the Icefield Ranges in general, was due to the Icefield Ranges Research Project, which was initiated jointly in 1961 by the Arctic Institute of North America and the American Geographical Society (Bushnell and Ragle, 1969, 1970, 1972, and Bushnell and Marcus, 1974).

Alsek River Valley System

The major glaciers of the Alsek hydrologic system in Canada are the Dusty [38 km long], Lowell [70 km], Fisher [48 km], Tweedsmuir [70 km], Vern Ritchie [46 km], Battle [27 km], and Melbern [20 km] Glaciers (fig. 1). The Alsek River cuts through the eastern part of the St. Elias Mountains and discharges into Dry Bay, Alaska. The surging glaciers in this group are the Dusty, Lowell, Fisher, and Tweedsmuir Glaciers (in sequence from the north), and all flow directly into the Alsek River valley.

Dusty Glacier surged about 1966; Lowell Glacier surged in 1948–50, in 1968–70, and in early 1983 (the last known surge). Dusty Glacier has a particularly simple, but distinctive, pattern of medial moraine loops, accentuated by a dark debris cover on the north side, which suggests that the north tributary is the surging one. An interesting through-flow of ice from the Dusty Glacier into the Lowell Glacier is also present, and this may be seen in figure 2, where it is evident from the transient snowline on both glaciers that Dusty Glacier is the higher of the two at that location. Also, it is possible to deduce from the ice structure and deformed or truncated medial moraines on Lowell Glacier that the flow is coming in from Dusty Glacier. On the 1:250,000-scale map sheet, this cannot be ascertained, but the newer (1987) 1:50,000-scale map (115B/8) shows the situation correctly. The deformed medial moraines on the lower part of Lowell Glacier are not easily interpreted. Post and others (1976) used easily identifiable points in the deformed moraine field, on successive images, to compute ice displacements between 1954 and 1973.

The next glacier south, Fisher Glacier, surged around 1970, but little information about this event is available. In 1973, Tweedsmuir Glacier began a surge (Holdsworth, 1973) that lasted only into early 1974. A quantitative analysis of glacier-surge dynamics using Landsat images of Tweedsmuir and Lowell Glaciers can be found in the separate section that follows. Tweedsmuir Glacier has a large piedmontlike lobe that expanded to dam the Alsek River temporarily in the winter of 1973–74. Because no flow was observed below the dam, the glacier ice must have been cold (that is, below 0°C). By the summer of 1974, the Alsek River was flowing past the glacier and caused massive ice calving into the river.

Glaciers in this group all have the potential for impeding the flow of the Alsek River, which has a peak summer discharge generally in the range 1,000–1,400 $m^3 s^{-1}$. Past surges of Lowell Glacier have been the most significant. Clague and Rampton (1982) documented the history of historic Lake Alsek, which formed several times during the past 1,000 years as a result of major damming of the Alsek River by Lowell Glacier. The last such event was thought to have been around 1900.

When these large historic lakes drained, they did so catastrophically and caused jökulhlaups downstream, as well as discharged meltwater and sediment into Dry Bay, Alaska. Evidence of these past floods is visible on the forested sides of the gorge between Fisher and Tweedsmuir Glaciers.

Quantitative Measurements of Tweedsmuir Glacier and Lowell Glacier Imagery

By Gerald Holdsworth, Philip J. Howarth, *and* C. Simon L. Ommanney

Introduction

Tweedsmuir and Lowell Glaciers (lat 59°52'N., long 138°19.3'W., and lat 60°17.8'N., long 138°17.2'W., respectively) are located in the St. Elias Mountains in the watershed of the Alsek River, a river that they both have

dammed in the recent past. The terminal regions of both glaciers exhibit prominent surface features typical of surging glaciers (Meier and Post, 1969). It is likely that their surges are, at least in part, thermally controlled (Clarke, 1976). Both glaciers are about 70 km long and average 1 km wide, although they are considerably wider in their terminal regions. One of the most distinctive aspects of their surface features is the folded structure seen in the exposed ice in the lower part of each glacier. The folds are defined by medial moraines and by different ice types, which may appear white, blue, or gray depending on the content of air bubbles and fine-grained sediment. The folds can clearly be identified on both terrestrial and aerial photographs (figs. 7 and 8) at most scales and very easily on Landsat images given favorable conditions. For the features to be seen on visible-band satellite images,

Figure 7.—*High-angle oblique aerial photograph of Tweedsmuir Glacier showing folded medial moraine loops and ice margin contact with the Alsek River. View is toward the south. Photograph no. 73R2–197 taken on 11 September 1973 by Austin Post, U.S. Geological Survey.*

the lower (ablation) region of the glacier, where the fold fields are found, needs to be totally free of seasonal snow cover. Because of this, and because of a high incidence of cloud cover in the region, the best period to obtain imagery to study moraine movement is normally in August or September, when, also, the low Sun angle provides optimum scene contrast and relief detail.

The two glaciers studied surge at slightly irregular intervals, typically, on average, at 20–30-year intervals, but not concurrently. During a surge, any preexisting curvilinear feature on the glacier will become folded because of nonhomogeneous strains in the ice. If surface folds are already present from a previous surge, they will be amplified during a subsequent surge. In addition to large longitudinal displacements, significant transverse displacements also result, which enable flow vectors (in two dimensions) to be obtained quite accurately. Employing conventional analyses of Landsat

Figure 8.—*High-angle oblique aerial photograph of Lowell Glacier showing complex structure in the medial moraines near the terminus. Icebergs can be seen in the proglacial lake. Alsek River flows south out of the lake toward the bottom of the picture. Photograph no. 69R1–287 taken on 25 August 1969 by Austin Post, U.S. Geological Survey.*

images, we used the spatial changes that took place in these surface fold fields over time to generate displacement, velocity, and strain-rate data. From these data, it is also possible to deduce something about the movement of the ice in the vertical direction.

By using Landsat images and aerial photographs, we studied Tweedsmuir Glacier during the late-surge (1973) and postsurge (1974) phases of a recent surge cycle. Lowell Glacier was studied in the presurge (1973–82) to the surge (1983) phase of the last surge cycle. From point-displacement measurements made on Landsat images taken about 5 years apart for Tweedsmuir Glacier and spanning about 10 years for Lowell Glacier, useful information relating to glacier-surge dynamics was obtained. In particular, the application of this information could be used to predict whether the Alsek River will be dammed again by a future surge of either glacier.

Observations on the Tweedsmuir Glacier Imagery

Tweedsmuir Glacier ends in an expanded lobe that is in contact with the Alsek River in several places during a surge. Its thickness has not been measured, but ice cliffs at the river valley contact were estimated to be about 25–30 m high in 1973. On the northern land-based sublobe, the cliff thickness was about 15 m. Thicknesses in the center of the lobe are probably about 50 to 100 m, based on marginal thicknesses, surface slopes, and the surrounding topographical detail seen on the 1:50,000-scale map sheets.

The glacier began to advance at its terminus in early 1973 (Holdsworth, 1973), possibly during April. Because surging evidently involves a series of linked processes, some delay may have been present before the ice edge actually began to move forward. The marginal ice was known to have been below the melting point, and hence, it was effectively frozen to the bedrock before the surge. During the surge, basal sliding and enhanced flow in any basal till would have been the most important mechanisms for ice transport. By direct observation, the peak activity would seem to have been in June or July 1973, and by the end of that year, the movement of the transient margin had decreased to very low levels. The speed of the ice flow in at least the lower 7 km of the glacier increased by about an order of magnitude during the surge (Post and others, 1976). This demonstrates the importance of basal sliding during a surge, a hypothesis further substantiated by Kamb and others (1985) in their study of the 1982–83 surge of Variegated Glacier, southeastern Alaska.

Krimmel and Meier (1975) show velocity vectors that indicate speeds in excess of 10 m d^{-1} between 22 July 1973 and 13 September 1973 in the same lower part of the glacier. These data were obtained from the Earth Resources Technology Satellite (ERTS-1, later renamed Landsat 1) satellite images that were enlarged to a scale of 1:50,000 and then analyzed by L.R. Mayo. Additional analyses were later done by Miller (1974).

In this paper, we are making types of measurements similar to these earlier ones, except that we used 1:25,000-scale plots obtained by processing digital Landsat data on a Canadian Image Analysis System (CIAS) at the Canada Centre for Remote Sensing in Ottawa. Enhanced and mutually registered electrostatic printer plots were produced for the excellent Landsat images of 13 September 1973 and 28 August 1978 (fig. 9), which cover the end of the surge and the postsurge period. The registration points used were all sufficiently far from the glacier to be safely assumed to be fixed. The same digital images at 1:50,000 scale registered acceptably with a 1:50,000-scale map compiled from 17 August 1974 vertical aerial photographs. Even if registration with a digital terrain map or a conventional map is not exact, registration between two satellite images of the same area is sufficient to provide acceptable displacement and, hence, velocity values for transient features in the scenes. Registration of the images was achieved by a least squares optical procedure that has a

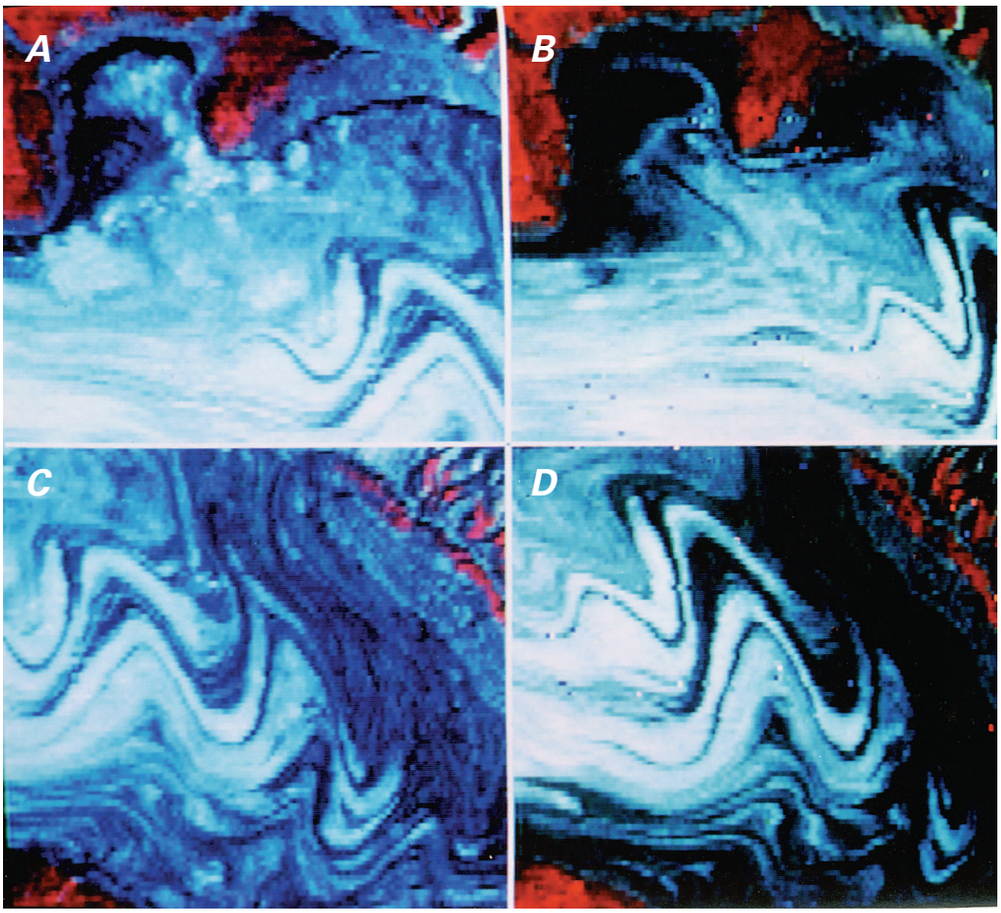

precision dictated by the picture element (pixel) dimension, approximately 57 m x 79 m. Displacements of the best defined points on the glacier were scaled directly from the registered transparencies and had an estimated error of between ±40 m and ±45 m.

Figure 9*A* shows very well the dark margin in 1973 on the north edge of the glacier caused by the 15-m high (and probably still advancing) ice cliff at that location. By 1978 (fig. 9*B*), this margin is poorly defined because of subsequent postsurge downwasting of the ice edge. Of great significance here is the observed displacement of the fold fields by 1978 (figs. 9*C*, *D*). The best measurement points in this area were mainly apices of folds. A total of 36 such points and 11 other miscellaneous points (of lesser reliability) were used to obtain a displacement field.

The resulting postsurge flow rates (fig. 10*A*) (~1 m d^{-1}) are seen to be about an order of magnitude less than the corresponding flow rates derived from L.R. Mayo's surge-phase data referred to earlier (Post and others, 1976, fig. 132). These findings are consistent with current knowledge of surge and intersurge behavior. Figure 10*B* is derived from figure 10*A* by generating 14 flow lines, starting at the left, that have equal (250-m) spacings. It was necessary to apply trial-and-error procedures in order to achieve a solution. The flow-line geometry illustrates the strongly divergent nature of the ice flow line in the terminal region. A similar conclusion was reached by L.R. Mayo from his earlier observations of the surge (see Krimmel and Meier, 1975).

Where sufficient velocity information is available along a particular flow line, or sufficiently close to it, as is the case for flow lines 5, 10, and 12 (fig. 10*B*), we computed longitudinal strain rates in a curvilinear coordinate system according to the equation:

$$\dot{\varepsilon}_{xx} = \Delta V_x / \Delta x \qquad (1)$$

where $\dot{\varepsilon}_{xx}$ is the time- and area-averaged longitudinal strain-rate compo-

Figure 9.—*Landsat 1 and 2 MSS false-color composite images of the north margin (***A*** and* ***B****) and the main fold field (***C*** and* ***D****) of Tweedsmuir Glacier showing changes that took place during the post-surge period.* A *and* C *are sections of a Landsat image (1417–19532; Path 65, Row 18) acquired on 13 September 1973, and* B *and* D *are sections of an image (21314–19295; Path 66, Row 18) acquired on 28 August 1978. The picture elements (pixels) measure approximately 57 m x 79 m. See figures 10*A*, 10*B*, 13*A*, and 13*B *for correct geographic orientation. Image was processed by Canada Centre for Remote Sensing, Ottawa, Ontario.*

nent of the total strain-rate tensor, and ΔV_x is the incremental change in the velocity component (V_x) over the distance Δx along the flow line. Lower order terms due to curvature are neglected.

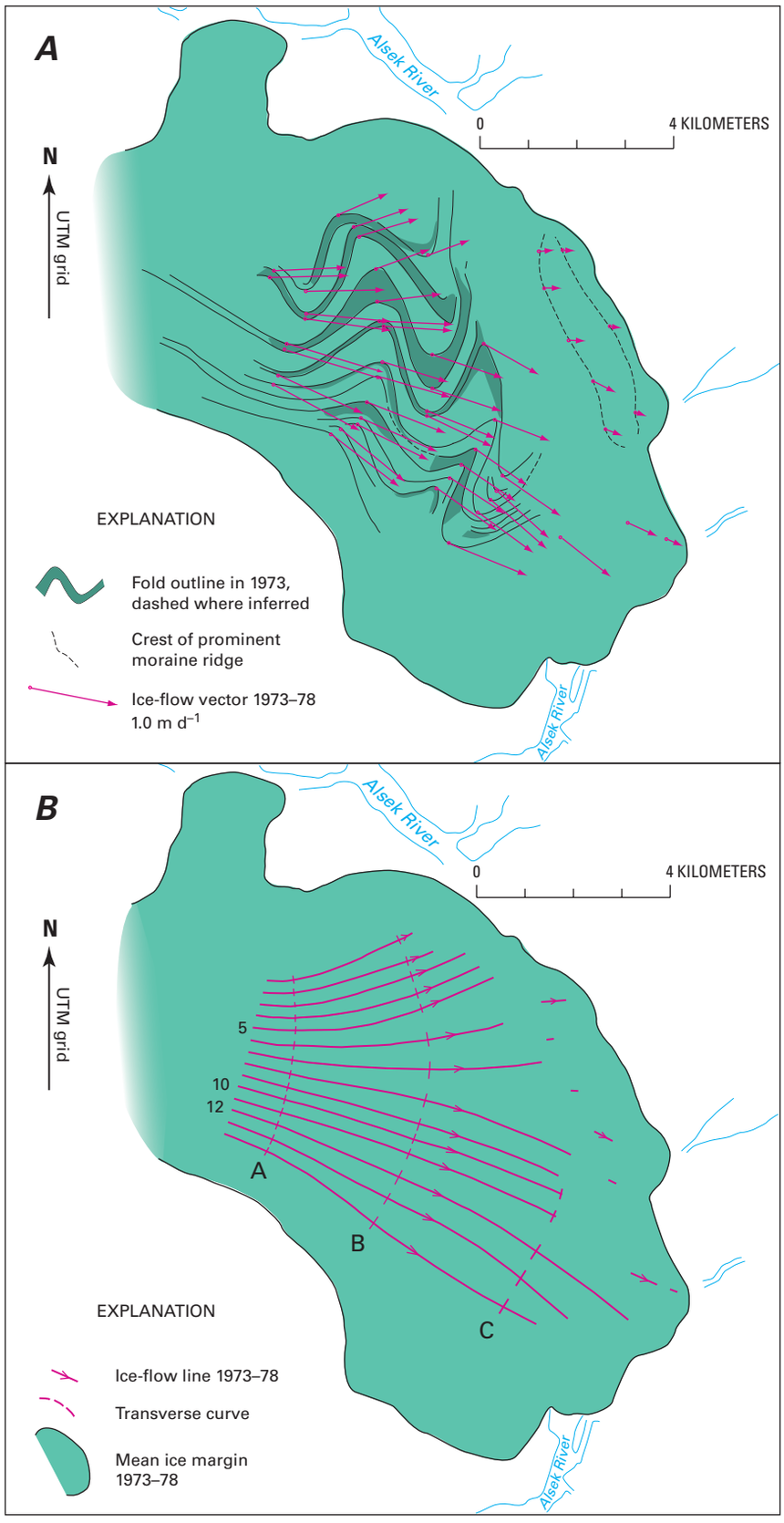

Figure 10.—*Tweedsmuir Glacier terminus showing ice-flow vectors and ice-flow lines for 1973–78.* **A**, *1973 fold geometry and ice-flow vectors based on analysis of the Landsat images shown in figure 9.* **B**, *Ice-flow lines based on the ice-flow vector field in* A. *Flow lines 5, 10, and 12 are discussed in the text, as are transverse curves A, B, and C.*

The time- and area-averaged transverse component of the strain-rate tensor $\dot{\varepsilon}_{yy}$ is obtained from the expression:

$$\dot{\varepsilon}_{yy} = W^{-1} V_x \Delta W / \Delta x \quad (2)$$

where, if we refer to a curvilinear cell defined by adjacent flow lines and the transverse curves labeled A, B, or C in figure 4*B*, W is the initial width of a cell, and $\Delta W / \Delta x$ is its gradient along the flow lines. V_x is the mean ice-flow rate along a flow line passing through the center of the cell. These flow rates are averaged over 2-km distances on much larger, smoothed curves of velocity versus distance.

So far, our analysis scheme has applied to two dimensions in the plane of the glacier surface, and as the reference frame moves with the surface (even vertically as ablation takes place), it is "Lagrangian" in character. It is possible to take advantage of a key property of glacier ice that allows us to infer what is happening in the direction perpendicular to the glacier surface. Because of the typically flat slopes of these glaciers in the ablation area (Clarke, 1991), this direction is approximately vertical.

The key property is the "incompressibility" of the ice, which allows us to write:

$$\Sigma \dot{\varepsilon}_{ii} = 0 \quad (3)$$

where $i = x, y, z$. This equation holds for any (orthogonal) reference-axis orientation and for ice of density near the maximum value of about 0.91 Mg m^{-3}.

Equation 3 expresses the conservation of volume and is used extensively in theoretical glaciology (Lliboutry, 1965; Paterson, 1994). From this equation, the vertical strain rate, $\dot{\varepsilon}_{zz}$, at a point can easily be calculated:

$$\dot{\varepsilon}_{zz} = -(\dot{\varepsilon}_{xx} + \dot{\varepsilon}_{yy}) \quad (4)$$

We will show later that our directions (x, y, z) correspond approximately to the principal axes of strain in the ice, so that we do not have to take the shear strains formally into account.

Results

Table 1 shows the values of $\dot{\varepsilon}_{xx}$, $\dot{\varepsilon}_{yy}$, and $\dot{\varepsilon}_{zz}$ computed from equations 1, 2, and 4 for selected points along flow lines 5, 10, and 12 (fig. 4*B*). Positive values indicate extension; negative values, contraction.

It may be seen that longitudinal compressive flow [down-glacier flow] is taking place consistently in this region of overall divergent flow [spreading flow, see Lliboutry, 1965, tome 2, p. 460–461]. Because of the large lateral creep, the vertical strain rate is consistently negative and indicates creep thinning (vertical compression), which is to be expected during the post-surge phase of a cycle. If we assume an ice thickness of 50 m, then for a mean vertical strain rate of –6 x 10^{-2} a^{-1}, the surface would be dropping by 3 m a^{-1}. This result is independent of any decrease in ice thickness that is caused by surface ablation, which could be of the same order.

We are not able to identify crevasse fields positively from the satellite imagery, but they may be seen on the excellent aerial photographs of Austin Post (fig. 7). These photographs show many splaying crevasses; that is, crevasses parallel to flow direction in the center but curving toward the

TABLE 1.—*Values of longitudinal, transverse, and vertical strain rates derived from analysis of Landsat images*[1]

Flow line	Longitudinal strain rate $\dot{\varepsilon}_{xx}(\pm 0.5 \times 10^{-2} a^{-1})$	Transverse strain rate $\dot{\varepsilon}_{yy}(\pm 0.5 \times 10^{-2} a^{-1})$	Vertical strain rate $\dot{\varepsilon}_{zz}(\pm 0.5 \times 10^{-2} a^{-1})$
5	–4.7	+18.3	–13.6
10	–6.1	+7.7	–1.6
12A	–2.6	+10.0	–7.4
12B	–1.8	+3.5	–1.7

[1] Errors given for values in the first two columns are not standard errors of a mean. They are derived through equation 1 and are the maximum for any flow line. The larger error in column two reflects the larger relative error in the transverse direction.

margin down the glacier. Splaying crevasses tend to be oriented along flow lines in the ablation area of spreading snouts (see, for example, Lliboutry, 1965). This result is consistent with the earlier assumption that the strain-rate components given in table 1 are probably close to the principal strain rates, which influence the direction of ice flow.

The strain-rate data in table 1 contrast with what would be expected during the surge phase. The longitudinal strain rates midway in 1973 may be estimated from some of the displacement data of L.R. Mayo (Krimmel and Meier, 1975). Between 22 July and 13 September 1973, along a section of the glacier corresponding to our flow line 7 (fig.10*B*), the vertical strain rates were between (+) 10^{-2} and 10^{-1} a^{-1}. This deduced thickening of the ice is consistent with our knowledge of peak surge behavior in the terminal region.

Observations on the Lowell Glacier Imagery

Lowell Glacier surged in 1983 after a quiescent phase of about 15 years. Conditions during the quiescent phase are documented in figures 11 and 12. From observations made by Parks Canada personnel and others, it is thought to have begun surging on or before middle April 1983. Figure 12 shows a synopsis of changes in the lower 30 km of the glacier between September 1973 and August 1983. The changes in the ice front (table 2), the changes in

Figure 11.—*Modified, digitally scanned reproduction of topographic map of Lowell Glacier, Yukon Territory. Map prepared by Gerald Holdsworth and D. Sherstone of the former Glaciology Subdivision, Inland Waters Directorate, Department of the Environment, from 17 August 1974 vertical aerial photographs. Contour interval on land, 100 m; contour interval on ice, 20 m. Original map scale, 1:50,000. Aerial photographs archived by the National Air Photo Library, Natural Resources Canada, Ottawa, Ontario. Goatherd Mountain, indicated by plus (+) symbol, is the ground-photograph station for figure 14. Abbreviations: UTM, Universal Transverse Mercator; N., north; E., east.*

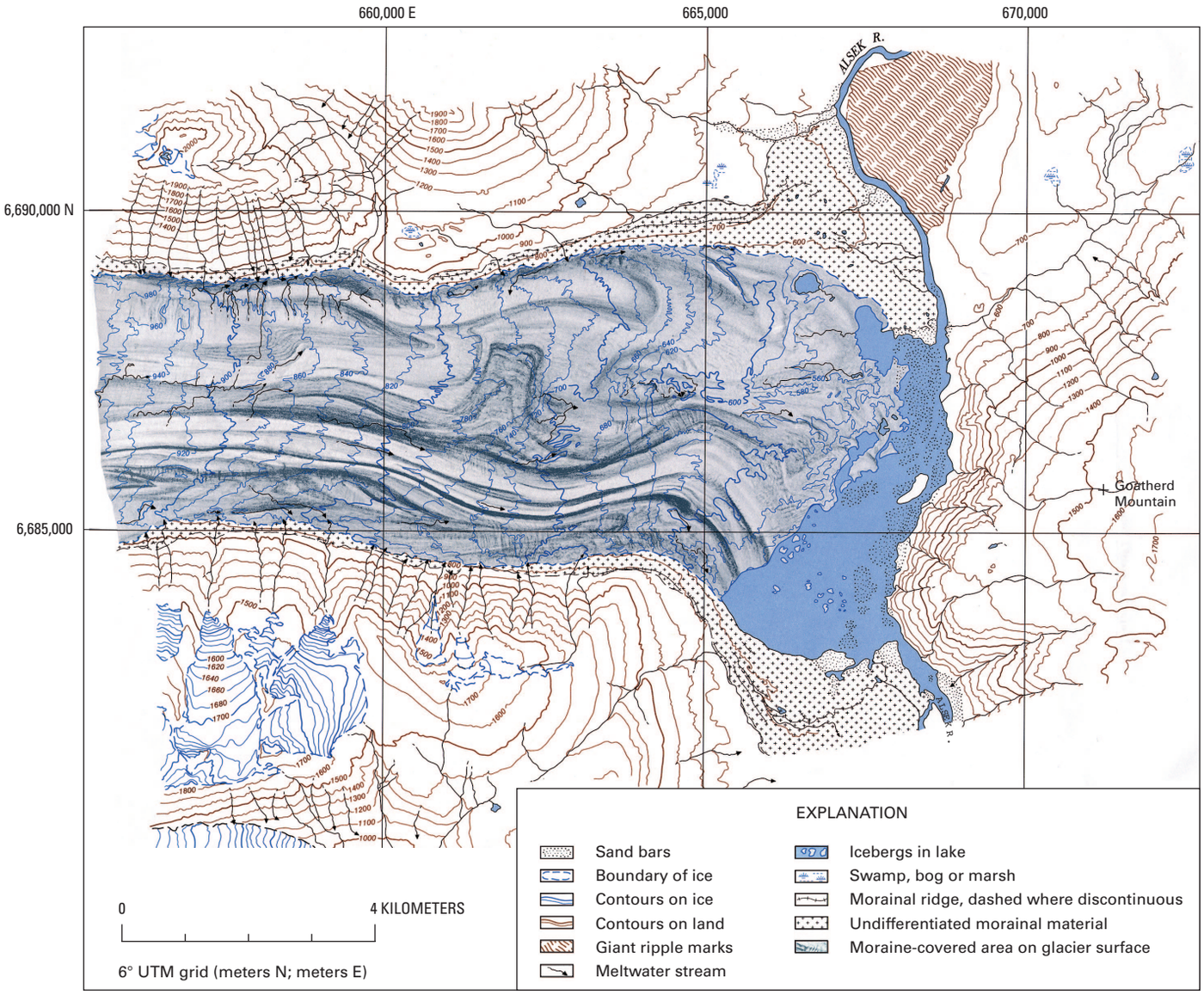

the lake area, and the development of dense clusters of icebergs can all be seen on the satellite imagery at the 1:1,000,000 scale; the images in figure 12 are annotated with these features. In interpreting the satellite images, we made extensive use of aerial and terrestrial photography. The 1983 images were interpreted with the help of terrestrial photographs taken by Lloyd Freese of Kluane National Park.

Figure 13 shows two Landsat 3 and 4 MSS (multispectral scanner) images taken on 23 June 1982 and 19 August 1983. In figure 13*A*, presurge

TABLE 2.—*Measurements of changes in the position of the terminus of the Lowell Glacier using Landsat imagery (see fig. 12)*

[Distances given are relative to the 13 September 1973 snout positions. —, not applicable. Abbreviations: ID no., identification number; N, North; S, South]

Date	Imagery	ID no.	Snout position change (meters)			Note
			N	Central	S	
13 Sep 1973	Landsat 1	1417–19532	—	—	—	Reference
17 Aug 1974	Aerial photographs	A23819/#50–60	—	—	—	Minor change
28 Aug 1978	Landsat 2	21314–19295	–2250	–500	–750	Retreat
17 Sep 1982	Landsat 4	Unknown	–2250	–2500	–2250	Retreat
9 Jun 1983	Landsat 4	40328–19482	–2050	–2000	–1450	Advance
19 Aug 1983	Landsat 4	40399–19540	–2050	–1250	–1050	Advance
28 Aug 1983	Landsat 4	40408–19475	–1250	–1000	–950	Advance

Figure 12.—*Lowell Glacier showing the changes in the geometry of the ice structure and margin from 1973 to 1983. The first three maps show presurge conditions. The second three show evidence of the surge. The maps were prepared from 1:500,000-scale photographic prints of Landsat images transferred to a 1:250,000-scale base map by the use of a Bausch and Lomb Zoom Transfer Scope. Fiducial marks are at 10–km spacing on the 6° UTM grid, zone 7 (see fig. 11). Symbols: L, lake water; B, icebergs; R, Alsek River. The Goatherd Mountain bluffs are shown shaded to the right in each map. Landsat images used for constructing each map are as follows:* **A**, *Landsat 1 (formerly ERTS–1) MSS image 1417–19532; 13 September 1973; Path 65, Row 18.* **B**, *Landsat 2 MSS image 21314–19295; 28 August 1978; Path 66, Row 18.* **C**, *Landsat 4 MSS image identification number unknown; 17 September 1982; Path 61, Row 18.* **D**, *Landsat 4 MSS image 40328–19482; 9 June 1983; Path 60, Row 18.* **E**, *Landsat 4 MSS image 40399–19540; 19 August 1983; Path 61, Row 18.* **F**, *Landsat 4 MSS image 40408–19475; 28 August 1983; Path 60, Row 18. The Landsat images are from the EROS Data Center, Sioux Falls, S. Dak.*

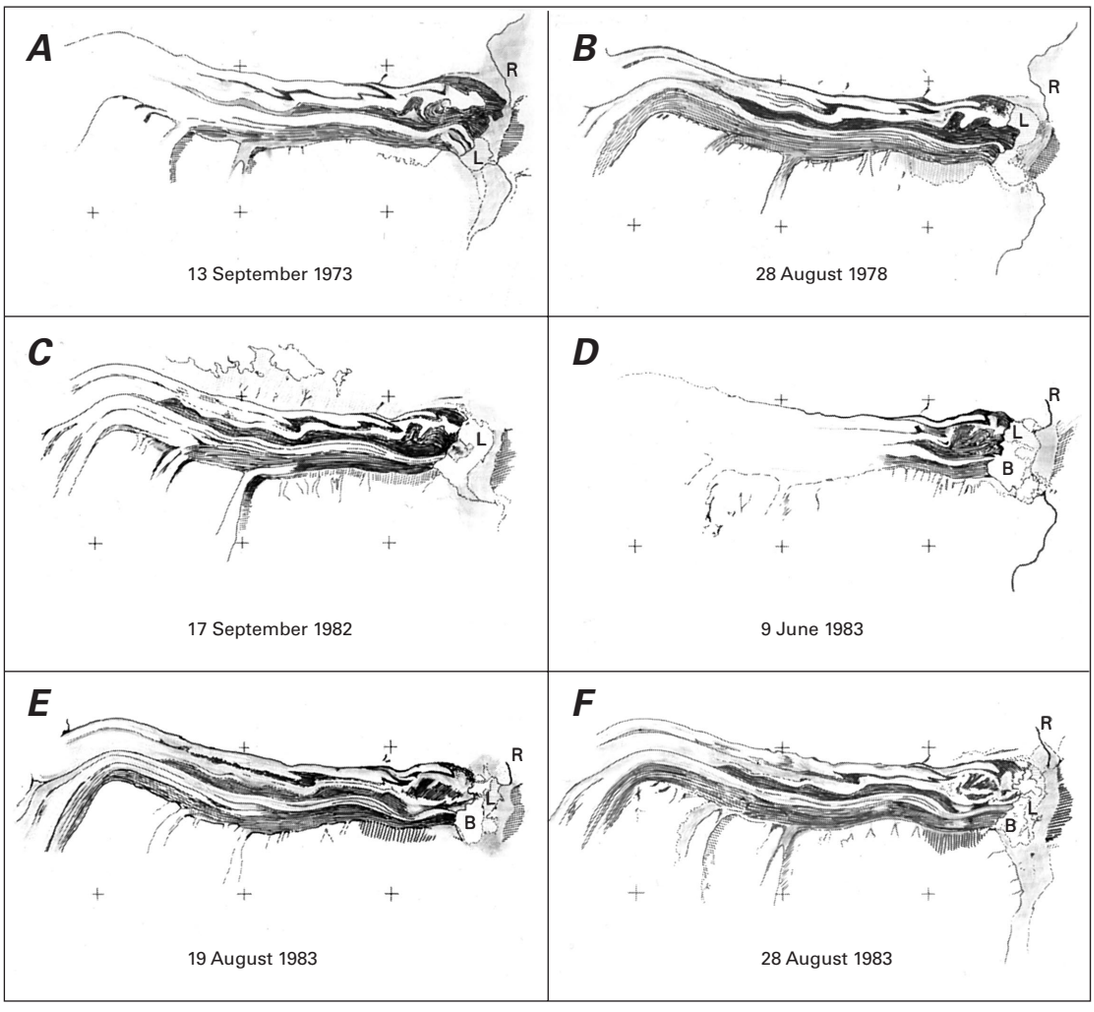

Figure 13.—*Landsat 3 and 4 MSS images of the Lowell Glacier showing conditions* **A** *just before and* **B** *during the 1983 surge. Dusty, Fisher, and Tweedsmuir Glaciers are also visible. The advance of the terminus is noticeable, and many icebergs are present in* B. *The Landsat images (*A, *31571–19514; 23 June 1982; Path 66, Row 18; and* B, *40399–19540; 19 August 1983; Path 61, Row 18) are from the EROS Data Center, Sioux Falls, S. Dak.*

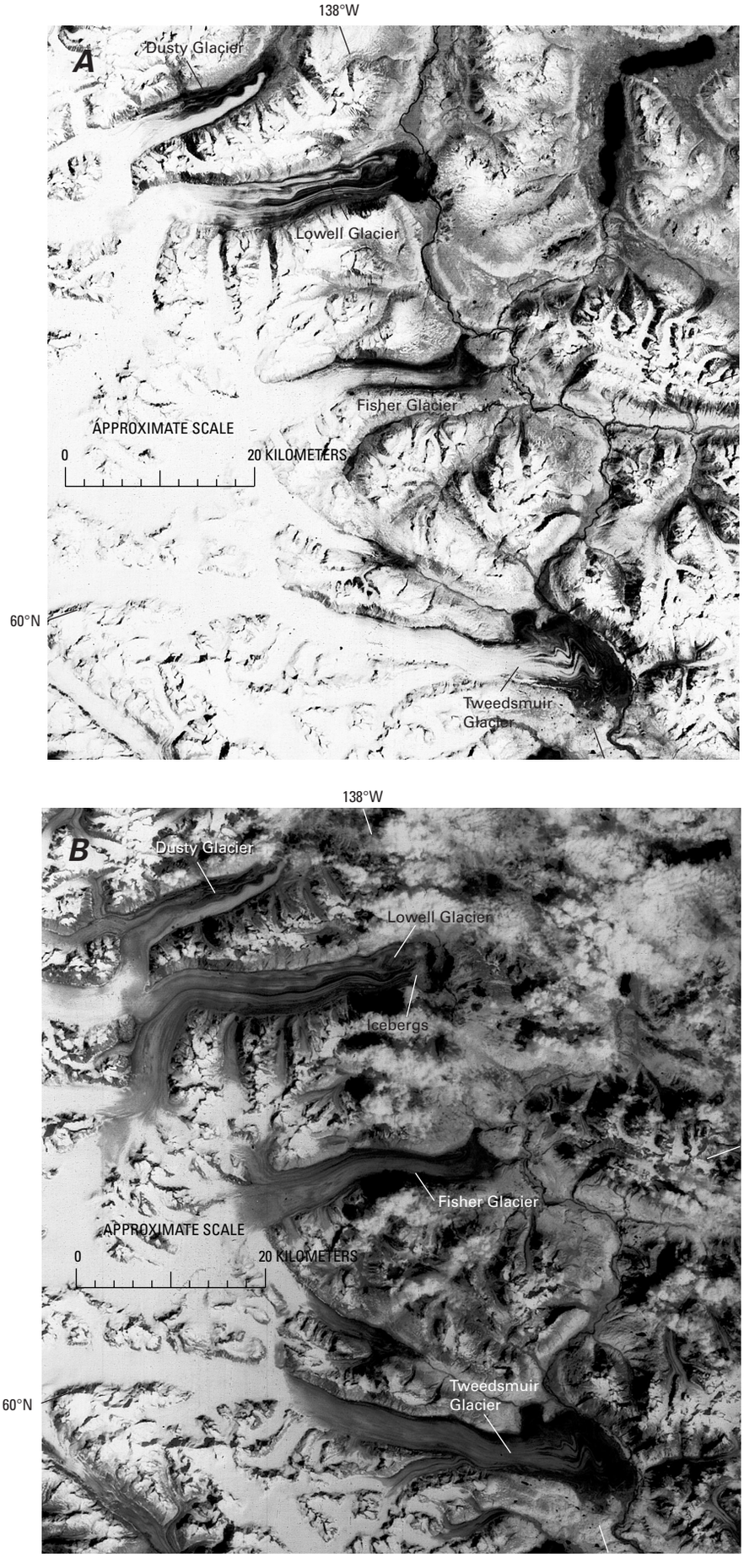

conditions apply, and in 13*B*, evidence of the surge can be seen, including a noticeable advance of the terminus. The existence of the proglacial lake and the river modify the terminal region to a great extent. The icebergs that cover the surface of the lake have an appearance similar to clouds. Observations of later satellite images (into 1984) and a visit to the glacier in summer 1984 (fig. 14) made it possible to predict that the ice front would not flow against Goatherd Mountain and dam the Alsek River, as had happened in earlier surges, perhaps as recently as near the beginning of the 20th century (Clague and Rampton, 1982).

In order to observe glacier behavior during a significant part of the quiescent phase (the previous, known surge was between 1968 and 1970), we have again selected excellent Landsat images of 13 September 1973 and 28 August 1978, enhanced the imagery, and prepared digital (Versatec) terrain plots of the glacier and adjacent areas. The plots were not mutually registered images, so in order to get acceptable registration for off-glacier reference points, we had to register the images by a visual iterative procedure for 10-km-square blocks per step. This, and the smaller relative displacements of Lowell Glacier for this period compared with Tweedsmuir Glacier, mean that less reliability can be placed on any velocity results from Lowell Glacier.

Figure 15*A* shows an array of easily identifiable reference points on the glacier surface. These were selected for the ice-displacement measurements. If we refer to figure 12, these points may be identified with prominent distortions of moraine bands or different (colored) ice types. Measurement of the displacement of these points was made between 1973 and 1978 by using the first two processed images in figure 12. For the following years, we used 1:500,000-scale photographic images transferred directly to the 1:250,000-scale NTS base map by the use of a Bausch and Lomb Zoom Transfer Scope. The results are shown in figure 15*B*, where the start of the (early) 1983 surge can be identified. [Note that some points were superior to others for making measurements, and in order to avoid interference of lines, not all the point displacements have been plotted. These points coincide with the center of each of the short vertical lines or error bars. These errors (~ ±45 m) are similar to the measurements made on Tweedsmuir Glacier and reflect pixel size, as well as errors due to "point" definition in different scenes.]

The average speed of each point (which is changing with position and time) is given by the slope of each curve at a given time. For the quiescent phase, 1973–82, the speeds decrease down the glacier from about 0.34 ± 0.03 m d^{-1} (point 1) to 0.04 ± 0.03 m d^{-1} (point 13). This indicates a general longitudinal compressive strain rate on the order of 10^{-2} a^{-1}, which is typical of many valley glaciers (Lliboutry, 1965). From a review of terrestrial photographs, a low rock knoll seen in figure 8 in August 1969 was apparently covered soon after and then uncovered again after 1973 in the

Figure 14.—*Two composite terrestrial photographs of the terminus of Lowell Glacier on 20 September 1984 showing the ice cliffs, Alsek River, flowing in from the right, and the transient lake containing some icebergs. Photograph by Gerald Holdsworth from Goatherd Mountain. See figure 11 for location of photograph station.*

region immediately down the glacier from the prominent "square" fold seen in the images. This knoll or *nunatak* was again overridden in the 1983 surge. The ice in this region is evidently quite thin.

During the surge, ice-flow rates increased to values of 12 m d^{-1} (curve 8, fig. 15*B*; point 8, fig. 15*A*) and 45 m d^{-1} (curve 1; point 1), representing an increase of more than two orders of magnitude above quiescent phase flow rates. Although some uncertainty exists in the magnitude of the errors in the last results (possibly up to 30 percent), they do seem to indicate a much greater relative increase in activity of the Lowell Glacier compared with the surge of Tweedsmuir Glacier a decade earlier.

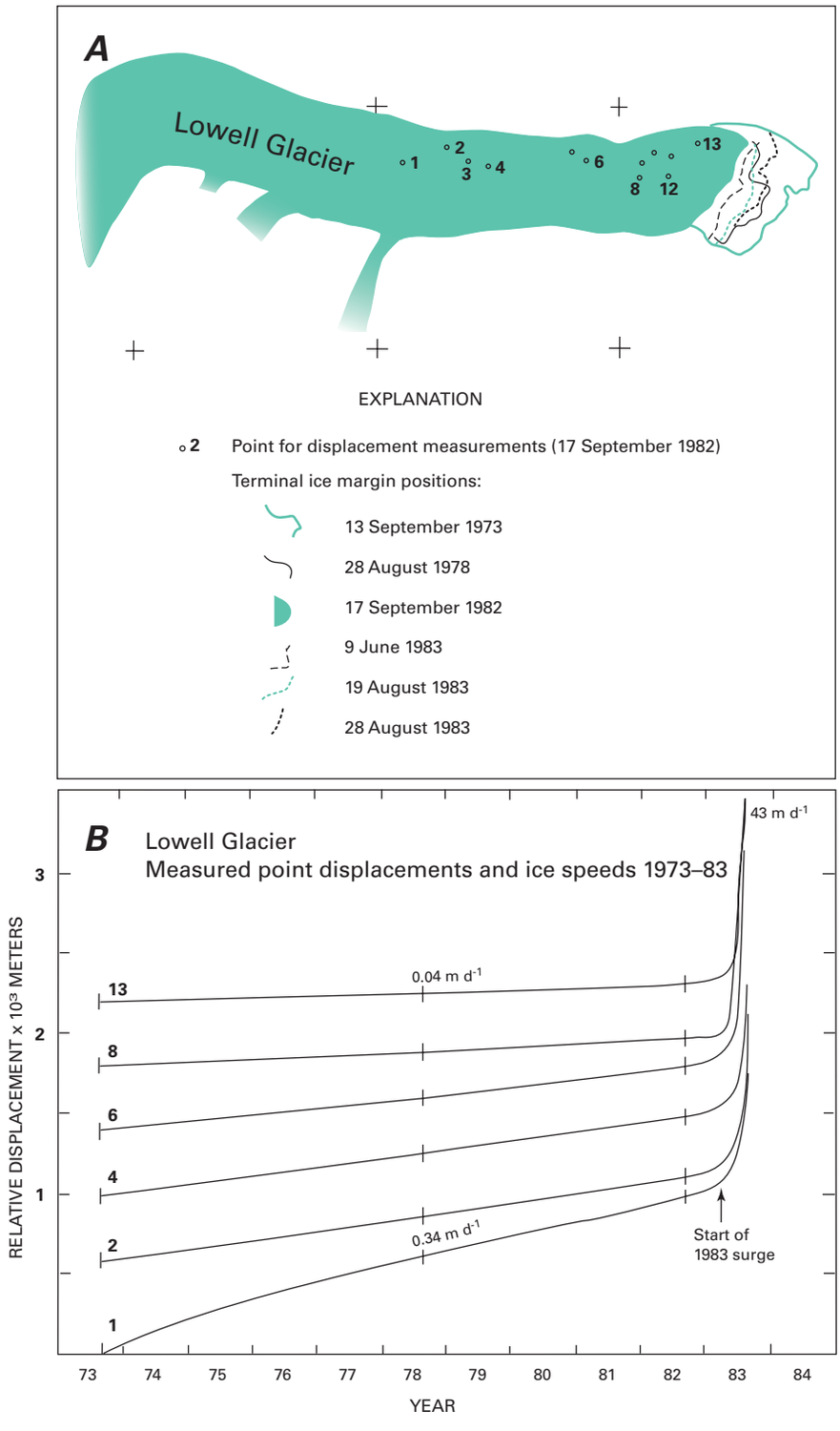

Figure 15.—*Terminal ice margin positions of the Lowell Glacier, relative point displacements, and ice speeds from 1973 to 1983.* **A**, *The location of terminal ice margin positions at different dates and the location of selected reference points on the glacier.* **B**, *The displacement versus time plots for six of the reference points shown in* A. *Errors in the displacement measurements are indicated by the length of the short vertical bars (estimated to be 90 m). Slopes of the curves give the ice speeds. Curve numbers in* B *correspond to point numbers in* A.

The unfavorable distribution of reference points, biased toward the north margin of the glacier (fig. 15*A*), and the lower accuracy of the registration for the Lowell Glacier have discouraged us from computing the components of the strain-rate tensor, as was done for Tweedsmuir Glacier. This deficiency is partially compensated by the excellent opportunity to determine longitudinal flow rates, which are biased toward the northern one-half of the glacier.

Value of Satellite Imagery

Significant information has been obtained about the dynamics of two large surging glaciers that occupy segments of a major Yukon-British Columbia-Alaska river system (the Alsek). This information has come from analysis of suitably selected Landsat imagery, supplemented by minimal ground-based observations. It is impractical to obtain such information in any other way (except by the much more expensive and time-consuming methods of aerial or terrestrial photogrammetry) because of the broken and dangerous nature of the glacier surface during a surge. (Even airborne radar does not work for determining ice thicknesses during a surge.) Satellite surveillance is also a practical way upon which to base predictions about potential hydrological hazards, such as jökulhlaups, that might result from the breaching of temporary ice dams of the Alsek River, as has happened several times in the past few centuries.

Seward Glacier Drainage System

Seward Glacier (labeled 17 in fig. 2) is actually an immense ice field of more than 1,200 km^2, the surface of which lies entirely in the accumulation area. This is the result of the extremely high snow-precipitation rate there. The glacier is temperate, and large crevasses are partially water filled in summer (Sharp, 1951a). Two major outlets come from the ice field: the narrow ice stream that feeds south into the vast Malaspina (Piedmont) Glacier (labeled 16 in fig. 2), which lies wholly in Alaska, and the Columbus Glacier (figs. 1 and 2), which feeds into the Bering Glacier, Alaska.

The spectacular medial moraine loops seen on the Malaspina Glacier are indicative of surging that can be traced to the outlet ice stream coming from Seward Glacier, and it is deduced that part of this system surges (Post, 1969).

In this glacier system, we will mention the ice-core sites on Mount Logan (labeled 1 in fig. 2), although hydrologically they properly should be placed in the Chitina River system, as most of the ice flowing from the upper plateau is to the north through Logan Glacier (labeled 3 in fig. 2). However, climatically, the sites are more aligned with the Pacific Ocean-Seward side of the mountain. The two sites are on the Northwest Col (5,340 m) and on the Prospectors-Russell Col (5,343 m), where 10-m firn temperatures are close to –29°C and –30°C, respectively. Ice thicknesses are generally between 100 and 200 m in the vicinity of the cols (saddles), although they increase out on the ice plateau, which has an area of about 15 km^2. Glaciological activities for the Northwest Col site are summarized in Holdsworth and others (1992). Information on the 2001-2 drilling project can be found at http://sts.gsc.nrcan.gc.ca/ice2001/home.asp.

Hubbard Glacier System

Hubbard Glacier [112 km] (labeled 18 in fig. 2) originates from a number of névés and divides that it shares with other valley glaciers (for example, Kaskawulsh and Logan Glaciers, labeled 12 and 3 in fig. 2, respectively). It flows across the Yukon-Alaska border [length to that point is 72 km] and ultimately calves into Yakutat Bay (fig. 1). The Alaskan section is discussed further in Chapter K, Glaciers of Alaska. Within Canada, the glacier appears to be wholly in the accumulation area. Geophysical studies on the Canadian part are restricted to the Hubbard-Kaskawulsh divide area, where the maximum firn-ice transition depth was found to be about 40 m. Ice depths are more than 500 m, and an ice-flow rate of 132 m a^{-1} was found about 10 km from the divide (Clarke, 1967). Glaciers on Mount Queen Mary (lat 60°37'N.; long 139°43'W.; 3,890 m; fig. 1) on the east side of the glacier are a source of lateral ice supply. In 1981, a surge was observed in one of the glaciers on the side of Mount Queen Mary, and a surge bulge moved out onto Hubbard Glacier. Areas of transient crevasse formation were often observed on the upper parts of Hubbard Glacier during the 1980's and early 1990's. Thus, even though the glacier is not formally identified as a surging glacier, it is dynamically very active, especially in its terminal region.

Grand Pacific-Melbern Glacier System

In the far southeastern part of the St. Elias Mountains, we find two interesting low-elevation transect glaciers that share a common divide at about 500 m above sea level. The south one of the pair is the Grand Pacific Glacier, well known for its numerous and apparently erratic oscillations across

***Figure 16**—Annotated Landsat 5 MSS mosaic of two images (Path 59, Row 19) showing the Grand Pacific, Ferris, and Melbern Glaciers, as well as other glaciers. Landsat images are from the EROS Data Center, Sioux Falls, S. Dak.*

the British Columbia-Alaska boundary (figs.1, 16). Following a catastrophic retreat up Tarr Inlet in the early part of the 20th century (see Chapter K, Glaciers of Alaska), its terminus retreated behind the border, where it stayed for several decades. In 1925, the (probably grounded) ice-front position was the farthest back on record, but by 1948, it had begun to approach the border, and by 1966, the ice front eventually extended at least 1 km into Alaskan waters before starting a steady retreat. By 1986, the ice front had retreated 0.8 km (Hall and others, 1995) but was still, barely, across the border in Alaska. Maps [for example, U.S. Operational Navigation Chart (ONC) D–12, scale 1:1,000,000] [all editions up to edition 6] typically show the ice front essentially coinciding with the border. Field (1958) [map 1.11] also shows the ice front coinciding with the border. The current status of the front has not been checked. Recent fluctuations have been connected with activity of the Ferris Glacier (fig. 16), one of the major tributaries of the Grand Pacific Glacier and probably a surging glacier.

On the other side of the divide, the situation is completely different. Melbern Glacier has generally thinned 300–600 m, and the terminus has retreated 15 km since the "Little Ice Age" maximum. About 7 km of this retreat took place between the middle 1970's and 1987 and caused the formation of one of the largest existing ice-dammed lakes. In 1987, the lake was full of tabular icebergs up to 200 m in diameter (Clague and Evans, 1994). Satellite imagery is particularly suitable for monitoring these types of major changes in Melbern Glacier, as well as in Grand Pacific Glacier.

References Cited

Bostock, H.S., 1969, Kluane Lake, Yukon Territory, its drainage and allied problems (155G and 115SE): Canada Geological Survey Paper 69–28, 19 p.

Bradbury, J.P., and Whiteside, M.C., 1980, Paleolimnology of two lakes in the Klutlan Glacier region, Yukon Territory, Canada: Quaternary Research, v. 14, no. 1, p. 149–168.

Brecher, H.H., 1966, Surface velocity measurements on the Kaskawulsh Glacier, Yukon Territory, Canada: Ohio State University Institute of Polar Studies Report 21, 73 p.

Bushnell, V.C., and Marcus, M.G., eds., 1974, Icefield Ranges Research Project scientific results: New York, American Geographical Society, and Montréal, Arctic Institute of North America, v. 4, 385 p.

Bushnell, V.C., and Ragle, R.H., eds., 1969, Icefield Ranges Research Project scientific results: New York, American Geographical Society, and Montréal, Arctic Institute of North America, v. 1, 224 p.

———1970, Icefield Ranges Research Project scientific results: New York, American Geographical Society, and Montréal, Arctic Institute of North America, v. 2, 139 p.

———1972, Icefield Ranges Research Project scientific results: New York, American Geographical Society, and Montréal, Arctic Institute of North America, v. 3, 263 p.

Clague, J.J., and Evans, S.G., 1994, Historic retreat of Grand Pacific and Melbern Glaciers, Saint Elias Mountains, Canada—An analogue for decay of the Cordilleran ice sheet at the end of the Pleistocene?: Journal of Glaciology, v. 40, no. 134, p. 205–210.

Clague, J.J., and Rampton, V.N., 1982, Neoglacial Lake Alsek: Canadian Journal of Earth Sciences, v. 19, no. 1, p. 94–117.

Clarke, G.K.C., 1967, Geophysical measurements on the Kaskawulsh and Hubbard Glaciers, Yukon Territory: Arctic Institute of North America Technical Paper 20, 36 p.

———1976, Thermal regulation of glacier surging: Journal of Glaciology, v. 16, no. 74, p. 231–250.

———1982, Glacier outburst floods from "Hazard Lake," Yukon Territory, and the problem of flood magnitude prediction: Journal of Glaciology, v. 28, no. 98, p. 3–21.

———1991, Length, width, and slope influence on glacier surging: Journal of Glaciology, v. 37, no. 126, p. 236–246.

Clarke, G.K.C., and Jarvis, G.T., 1976, Post-surge temperatures in Steele Glacier, Yukon Territory, Canada: Journal of Glaciology, v. 16, no. 74, p. 261–268.

Clarke, G.K.C., and Mathews, W.H., 1981, Estimates of the magnitude of glacier outburst floods from Lake Donjek, Yukon Territory, Canada: Canadian Journal of Earth Sciences, v. 18, no. 9, p. 1452–1463.

Collins, S.G., and Clarke, G.K.C., 1977, History and bathymetry of a surge-dammed lake: Arctic, v. 30, no. 4, p. 217–224.

Dewart, Gilbert, 1970, Seismic investigation of the ice properties and bedrock topography at the confluence of the north and central arms of the Kaskawulsh Glacier, *in* Bushnell, V.C., and Ragle, R.H., eds., Icefield Ranges Research Project scientific results: New York, American Geographical Society, and Montréal, Arctic Institute of North America, v. 2, p. 77–102.

Driscoll, F.G., Jr., 1980, Formation of the neoglacial surge moraines of the Klutlan Glacier, Yukon Territory, Canada: Quaternary Research, v. 14, no. 1, p. 19–30.

Field, W.O., 1958, Atlas of mountain glaciers in the Northern Hemisphere: Natick, Mass., Quartermaster Research and Engineering Command, Headquarters, U.S. Army Technical Report EP 92, unpaginated.

———ed., 1975, Mountain glaciers of the Northern Hemisphere: Hanover, N.H., U.S. Army Corps of Engineers, Cold Regions Research and Engineering Laboratory, v. 2, 932 p.

Hall, D.K., Benson, C.S., and Field, W.O., 1995, Changes of glaciers in Glacier Bay, Alaska, using ground and satellite measurements: Physical Geography, v. 16, no. 1, p. 27–41.

Holdsworth, Gerald, 1965, An examination and analysis of the formation of transverse crevasses, Kaskawulsh Glacier, Yukon Territory, Canada: Ohio State University Institute of Polar Studies Report 16, 90 p.

———1973, Surge of Tweedsmuir Glacier, British Columbia, Canada: Ice, no. 43 (3d issue), p. 23.

———1992, Ice cores as a source of long-term net precipitation data—A North American perspective, *in* Kite, G.W., and Harvey, K.D., eds., Using hydrometric data to detect and monitor climatic change: National Hydrology Research Institute Symposium 8, Saskatoon, Saskatchewan, 1992, p.107–120.

Holdsworth, Gerald, Krouse, H.R., and Nosal, M., 1992, Ice core climate signals from Mount Logan, Yukon, A.D. 1700–1987, *in* Bradley, R.S., and Jones, P.D., eds., Climate since A.D. 1500: New York, Routledge, p. 483–504.

Holdsworth, Gerald, and Peake, E., 1985, Acid content of snow from a mid-troposphere sampling site on Mt. Logan, Yukon Territory, Canada: Annals of Glaciology, v. 7, p. 153–160.

Jackson, J.A., ed., 1997, Glossary of geology (4th ed.): Alexandria, Va., American Geological Institute, 769 p.

Jarvis, G.T., and Clarke, G.K.C., 1974, Thermal effects of crevassing on Steele Glacier, Yukon Territory, Canada: Journal of Glaciology, v. 13, no. 68, p. 243–254.

———1975, The thermal regime of Trapridge Glacier and its relevance to glacier surging: Journal of Glaciology, v. 14, no. 71, p. 235–250.

Johnson, P.G., 1972a, A possible advanced hypsithermal position of the Donjek Glacier: Arctic, v. 25, no. 4, p. 302–305.

———1972b, The morphological effects of surges of the Donjek Glacier, St. Elias Mountains, Yukon Territory, Canada: Journal of Glaciology, v. 11, no. 62, p. 227–234.

Kamb, B., Raymond, C.F., Harrison, W.D., Engelhardt, Hermann, Echelmeyer, K.A., Humphrey, N., Brugman, M.M., and Pfeffer, T., 1985, Glacier surge mechanism, 1982–83 surge of Variegated Glacier, Alaska: Science, v. 227, no. 4686, p. 469–479.

Krimmel, R.M., and Meier, M.F., 1975, Glacier applications of ERTS images: Journal of Glaciology, v. 15, no. 73, p. 391–402.

Lliboutry, Louis, 1965, Traité de glaciologie, tome 2: Glaciers, variations du climat, sols gelés [Treatise of glaciology, v. 2: Glaciers, climatic variations, and frozen ground]: Paris, Masson et Cie, 612 p.

Meier, M.F., and Post, Austin, 1969, What are glacier surges?: Canadian Journal of Earth Sciences, v. 6, no. 4, pt. 2, p. 807–817.

Miller, J.M., 1974, Environmental surveys in Alaska based upon ERTS data, *in* Freden, S.C., Mercanti, E.P., and Friedman, D.B., eds., Third Earth Resources Technology Satellite Symposium, II: U.S. National Aeronautics and Space Administration Special Publication 356, p. 12–40.

Paterson, W.S.B., 1994, The physics of glaciers (3d ed.): Oxford, U.K., Elsevier Science, 480 p.

Post, Austin, 1966, The recent surge of Walsh Glacier, Yukon and Alaska: Journal of Glaciology, v. 6, no. 45, p. 375–381.

———1967, Walsh Glacier surge, 1966 observations: Journal of Glaciology, v. 6, no. 47, p. 763–765.

———1969, Distribution of surging glaciers in western North America: Journal of Glaciology, v. 8, no. 53, p. 229–240.

Post, Austin, Meier, M.F., and Mayo, L.R., 1976, Measuring the motion of the Lowell and Tweedsmuir surging glaciers of British Columbia, Canada, *in* Williams, R.S., Jr., and Carter, W.D., eds., ERTS–1, a new window on our planet: U.S. Geological Survey Professional Paper 929, p. 180–184.

Rampton, V.N., 1970, Neoglacial fluctuations of the Natazhat and Klutlan Glaciers, Yukon Territory, Canada: Canadian Journal of Earth Sciences, v. 7, no. 5, p. 1236–1263.

Sharp, R.P., 1943, Geology of the Wolf Creek area, St. Elias Range, Yukon Territory, Canada: Geological Society America Bulletin, v. 54, no. 5, p. 625–650.

Sharp, R.P., 1951a, Glacial history of Wolf Creek, St. Elias Range, Canada: Journal of Geology, v. 59, no. 2, p. 97–117.

———1951b, Thermal regimen of firn on upper Seward Glacier, Yukon Territory, Canada: Journal of Glaciology, v. 1, no. 9, p. 476–487.

Stanley, A.D., 1969, Observations on the surge of Steele Glacier, Yukon Territory, Canada: Canadian Journal of Earth Sciences, v. 6, no. 4, pt. 2, p. 819–830.

Whiteside, M.C., Bradbury, J.P., and Tarapchak, S.J., 1980, Limnology of the Klutlan moraines, Yukon Territory, Canada: Quaternary Research, v. 14, no. 1, p. 130–148.

Wood, W.A., 1936, The Wood Yukon expedition of 1935—An experiment in photographic mapping: Geographical Review, v. 26, no. 2, p. 228–246.

———1942, The parachuting of expedition supplies—An experiment by the Wood Yukon expedition of 1941: Geographical Review, v. 32, no. 1, p. 36–55.

———1972, Steele Glacier, 1935–1968, *in* Bushnell, V.C., and Ragle, R.H., eds., Icefield Ranges Research Project scientific results: New York, American Geographical Society, and Montréal, Arctic Institute of North America, v. 3, p. 1–8.

Wright, H.E., Jr., 1980, Surge moraines of the Klutlan Glacier, Yukon Territory, Canada—Origin, wastage, vegetation succession, lake development, and application to the late-glacial of Minnesota: Quaternary Research, v. 14, no. 1, p. 2–18.